THE JOURNAL OF PHYSICAL CHEMISTRY C

Article

pubs.acs.org/JPCC

Insight into Hydrogen Bonding of Uranyl Hydroxide Layers and Capsules by Use of ^{1}H Magic-Angle Spinning NMR Spectroscopy

Todd M. Alam,*[,†] Zuolei Liao,[‡] May Nyman,[‡] and Jonathan Yates[§]

[†]Department of Organic Material Science, Sandia National Laboratories, Albuquerque, New Mexico 87185, United States

[‡]Department of Chemistry and Materials, Oregon State University, Corvallis, Oregon 97331, United States

[§]Department of Materials, University of Oxford, Oxford OX1 3PH, United Kingdom

Supporting Information

ABSTRACT: Solid-state ^{1}H magic-angle spinning (MAS) NMR was used to investigate local proton environments in anhydrous $[UO_2(OH)_2]$ (α-UOH) and hydrated uranyl hydroxide $[(UO_2)_4O(OH)_6{\cdot}5H_2O$ (metaschoepite). For the metaschoepite material, proton resonances of the μ_2-OH hydroxyl and interlayer waters were resolved, with two-dimensional (2D) double-quantum (DQ) ^{1}H−^{1}H NMR correlation experiments revealing strong dipolar interactions between these different proton species. The experimental NMR results were combined with first-principles CASTEP GIPAW (gauge including projector-augmented wave) chemical shift calculations to develop correlations between hydrogen-bond strength and observed ^{1}H NMR chemical shifts. These NMR correlations allowed characterization of local hydrogen-bond environments in uranyl U_{24} capsules and of changes in hydrogen bonding that occurred during thermal dehydration of metaschoepite.

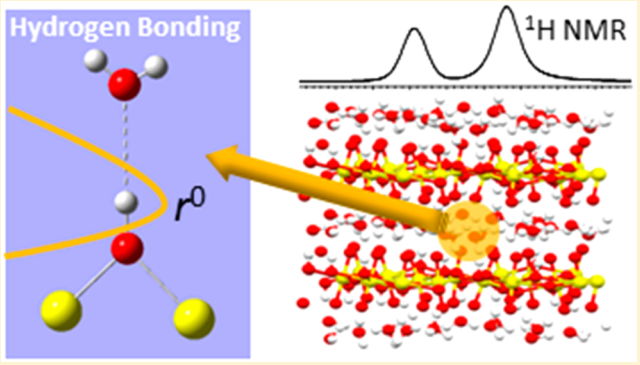

1. INTRODUCTION

Successful stewardship of uranium-based fuels and generated waste remains a major challenge for nuclear energy use and development.[1] The solution speciation and structure of different UO_2- and UOH-containing phases ultimately controls the chemistry of uranium processing and extraction in various steps of the nuclear fuel cycle, as well as transport and biomineralization precipitation of uranium in natural settings.[2] For example, aqueous corrosion of UO_2-related waste can produce multiple phases based on the differential presence of heat, water, radiation, or oxidizing conditions.[3] For sufficiently high uranium concentrations under neutral pH conditions, U(VI) precipitates as schoepite, which can partially dehydrate to form metaschoepite.[4] Distinction between schoepite, metaschoepite, and dehydrated schoepite is still unresolved, as there is easy conversion between the three variations of these closely related phases in natural and laboratory settings, and they are usually present as a mixture. For uranium oxide hydrates of the form $UO_3{\cdot}nH_2O$, the reported crystal structures are composed of UO_2^{2+} cations with linking O and OH groups forming a continuous polyhedral layer of $(UO_2)_4O(OH)_6$ with UO_7 pentagonal bipyramids separated by a layer of H_2O (Figure 1A). Schoepite (n = 2.25) is described by $(UO_2)_8O_2(OH)_{12}{\cdot}12H_2O$ composition,[5,6] while metaschoepite (n = 2) loses two waters to become $(UO_2)_4O(OH)_6{\cdot}5H_2O$.[7] The interlayer waters are disordered over different symmetry sites but are involved in both interwater hydrogen bonding and hydrogen bonding with the bridging hydroxyl (μ_2-OH). Further dehydration of metaschoepite leads to different phases reported as "dehydrated schoepite", (UO_2)-$O_{0.25-x}(OH)_{1.25+2x}$,[4,8] or the related mineral paulscherrerite, $UO_2(OH)_2$.[8] These dehydrated schoepite materials are closely related to the uranyl hydroxide α-UOH. They are chemically described as $UO_2(OH)_2$, with a structure consisting of an infinite sheet of corner-linked octahedral UO_6 and μ_2-OH hydroxyls forming hydrogen bonds to the adjacent layer U═O oxygens (Figure 1B).[9] Subsequent dehydration, oxidation, or complexation with other cations/anions leads to a variety of other uranyl phases.[10−14]

Crystal structures for many of the hydrated uranyl materials have proton positions that are not resolved (or are highly disordered), making it important to develop additional experimental techniques that probe the local proton environments. To characterize hydrated uranyl oxides, different experimental methods including extended X-ray absorption fine structure (EXAFS), X-ray, Raman, and nuclear magnetic resonance (NMR) spectroscopies have been utilized.[4−6,10,15,16] The majority of the NMR experiments are solution-phase studies of monomers and clusters related to the uranyl materials and are predominantly ^{17}O NMR investigations involving

Received: March 15, 2016
Revised: April 25, 2016
Published: April 27, 2016

DOI: 10.1021/acs.jpcc.6b02692
J. Phys. Chem. C 2016, 120, 10675−10685

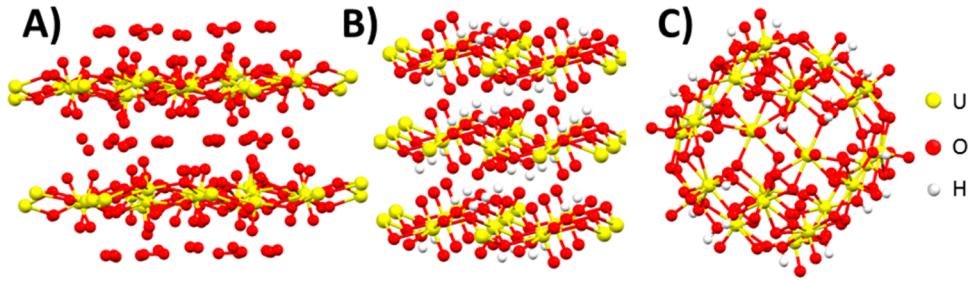

Figure 1. Crystal structures of layered uranyl hydroxides: (A) metaschoepite, $(UO_2)_4O(OH)_6{\cdot}5H_2O$; (B) α-UOH, $UO_2(OH)_2$; and (C) U_{24} uranyl peroxide/hydroxide capsule, $[UO_2(O)_2(OH)]_{24}^{24-}$. Water and hydroxyl proton positions in the crystal structure of metaschoepite have not been reported.

oxygen speciation and quantification of oxygen exchange rates within uranium coordination environments.[15−19] Additionally, ^{133}Cs and ^{23}Na solution NMR of cation dynamics in related uranyl peroxide/hydroxide capsulelike clusters[20,21] and ^{1}H and ^{13}C NMR of different carbonate, carboxylic acid, and amino acid ligands complexing uranyl monomers and small oligomers have been exploited.[10,11,13,18,19,22,23] Solid-state NMR studies have been more limited but do include the classic static wide-line ^{1}H NMR investigations of water rotational dynamics in $UO_3{\cdot}nH_2O$ phases.[24−27] By careful analysis of the second moment of the ^{1}H NMR spectral line shape, these authors determined that a portion of the protons in these uranyl phases were not associated with water. Instead they were assignable to hydroxyl protons, even though there was no resolution in the static NMR spectra. The improved resolution afforded by magic-angle spinning (MAS) NMR to further investigate uranyl materials has been demonstrated. Example include ^{1}H and ^{133}Cs MAS NMR of uranyl silicates;[14,28] ^{1}H, ^{7}Li, ^{23}Na, and ^{133}Cs MAS NMR studies of cation dynamics in uranyl peroxide/hydroxide capsules $[UO_2(O)_2(OH)]_{24}^{24-}$ (U_{24}) and $[UO_2(O)_{1.5}]_{28}^{28-}$ (U_{28});[21,29] and more recently, ^{1}H and ^{17}O MAS NMR of studtite $(UO_2)(O_2)(H_2O)_2](H_2O)_2$, amorphous U_2O_7, and metaschoepite.[30] In the U_{24} capsule studies, solid-state NMR results were utilized in an effort to corroborate solution behavior and dynamics as well as gain a more complete understanding of these unique structures.

For U_{24} uranyl capsules, the hydroxide ligand (OH) bridges two uranyl centers, with the H-atom position not readily determined by single-crystal X-ray diffraction. It was assigned as a hydroxyl rather than an oxo ligand on the basis of charge-balancing requirements, bond valence sum, and bond length. Recent computational studies suggest the OH ligand is pointing outward from the capsule, as we would expect from the curvature and resulting U(OH)U bond angle (see Figure 1C).[31] However, no spectroscopic techniques have adequately characterized these hydroxyl ligands. Even Raman spectroscopic data have led to some disagreement in the literature concerning assignment of the characteristic OH vibrational band.[32,33] While the OH ligand cannot be observed by solution ^{1}H NMR (likely due to exchange broadening), it is easily detected by solid-state NMR.[29] In ^{1}H MAS NMR investigations of U_{24} materials, multiple resonances having large chemical shifts (>10 ppm) were reported. The shift varies with both cation speciation and capsule size.[29] These observations provided motivation to study simple uranyl hydroxide phases, both hydrated and nonhydrated, to obtain benchmark ^{1}H NMR characterization of the μ_2-OH(U_2) hydroxyl ligand bridging two uranyl centers, as this ligand is a common structural motif in uranyl peroxide capsules.[34] In this paper, our recent efforts using moderate spinning speed (~25 kHz) ^{1}H MAS NMR to characterize water and hydroxyl proton environments in metaschoepite and α-UOH are presented. ^{1}H MAS NMR allows the hydrogen-bond network between the interlayer waters and between water and the bridging hydroxyl species to be probed (see also Scheme 1 for a generalized representation of hydrogen-bond motifs). Using first-principles GIPAW (gauge including projector-augmented wave) NMR chemical shift calculations, correlations between observed ^{1}H MAS NMR chemical shift and hydrogen-bond strength were developed. These correlations were first performed for simple layered uranyl hydroxide materials and then extended to more complex uranyl peroxide/hydroxide capsules.

2. EXPERIMENTAL DETAILS

2.1. Preparation of Uranyl Hydroxides.

Caution! Uranium is radioactive and hazardous and should only be prepared and handled in laboratories where Environmental Safety and Health training and engineered safety protocols for uranium operations have been established. Uranyl nitrate (depleted) was acquired from Fluka Chemical Corp. and recrystallized from hot water prior to use. All other chemicals were used as received without further purification. The $[\alpha$-$UO_2(OH)_2]$ (α-UOH for brevity) was synthesized via the procedure reported by Dawson et al.[35] Uranyl nitrate (0.5 g) was dissolved in 10 mL of distilled water and then added to 1.0 mL of 30% H_2O_2 dissolved in 10 mL of water while stirring. The yellow precipitate was isolated by centrifugation, washed with water six times, and then dried under vacuum at room temperature. The dried yellow solid was then transferred into an alumina crucible and heated to 375 °C with a 10 °C/min ramp in air for 1 h. The resulting yellow-orange solid was then sealed in a Parr Teflon reaction vessel along with 12 mL of water and heated to 230 °C for 72 h. The final product (0.24 g) was recovered as small yellow crystals via filtration with 80% uranium yield. The metaschoepite material $[(UO_2)_4O(OH)_6{\cdot}5H_2O]$ was prepared from a 0.1 M uranyl nitrate stock solution made by dissolving 0.78 g of crystalline uranyl nitrate in 15 mL of water. This was followed by diluting 3.0 mL of the stock solution with an additional 5 mL of distilled water. This solution was then heated to 75 °C in a water bath while 0.4 mL of 4 M $NH_3{\cdot}H_2O$ was added with stirring. The yellow cloudy mixture was transferred into a 20 mL Parr Teflon reaction vessel along with 3 mL of additional water for hydrothermal treatment at 140 °C for 72 h. The final product (0.057 g) was recovered as a yellow powder via filtration, giving a yield of 59%. Although we could not obtain absolutely pure schoepite or metaschoepite, since these forms interconvert dynamically (with atmospheric

DOI: 10.1021/acs.jpcc.6b02692
J. Phys. Chem. C 2016, 120, 10675−10685

exposure, heat, etc.), any mixture thereof serves as a model layered hydrated uranyl hydroxide phase, that for the purposes of this study can be compared to anhydrous $[UO_2(OH)_2]$. As described below, our material is predominantly metaschoepite, so for simplicity, it is referred to as such throughout the text. These materials were packed in uranyl-designated 2.5 mm MAS rotors in a radioactive control laboratory prior to NMR analysis. The metaschoepite heating experiments were performed directly on materials in the MAS rotors. The rotor end-caps were removed, followed by placement of the filled rotor into an oven for a targeted temperature and time. The rotors were then cooled and sealed by replacement of the caps, followed by NMR analysis. Heat treatments were cumulative, as only a single sample was available for NMR analysis. This in-rotor heating procedure was implemented to retain the very small amounts of the uranyl materials (~10 mg), since material loss was expected to occur during the repeated unpacking/packing of the MAS NMR rotor and to reduce the amount of external uranium contamination of rotors or equipment occurring during the heating process.

2.2. Material Characterization. Powder X-ray diffraction (XRD) patterns were recorded on a Rigaku Ultima IV diffractometer using Cu Kα radiation of 0.154 18 nm. Raman spectra were recorded on a Thermo Scientific DXR spectrometer with 760 nm laser source. Thermogravimetric analysis (TGA)/differential scanning calorimetry (DSC) data were recorded on a TA Instruments SDT Q 600 under air flow. Solid-state ^{1}H MAS NMR spectra were obtained on a Bruker Avance III instrument operating at 600.14 MHz, using a 2.5 mm broadband probe spinning between 20 and 25 kHz, unless otherwise noted. ^{1}H chemical shifts were referenced to the solid external secondary sample adamantane at δ = +1.63 ppm with respect to tetramethylsilane (TMS) δ = 0.0 ppm. It is known that, for high spinning speeds, significant frictional heating occurs. The actual sample temperatures were calibrated with the ^{207}Pb chemical shift change of a secondary $Pb(NO_3)_2$ sample,[36,37] and are noted in the paper. The two-dimensional (2D) double-quantum (DQ) ^{1}H MAS correlation experiments utilized the chemical shift and offset compensated back-to-back (BABA) multiple pulse sequence for excitation and reconversion of the multiple quantum coherences.[38] Phase-sensitive detection in the F_1 dimension was obtained by the States time-proportional phase incrementation (TPPI) method. Spectral deconvolutions were performed by use of the DMFIT software package.[39]

2.3. Chemical Shift Calculations and Small Cluster Optimizations. Coordinates of the single relaxed metaschoepite structure used for the chemical shift calculations were graciously provided by Professor Ostanin and were produced by molecular dynamics (MD) methods as previously described.[40] The starting MD configuration was based on the crystal structure of schoepite where each unit cell is composed of 8 U atoms, 24 O atoms, and 18 H_2O groups. Atom positons were optimized prior to the start of the simulations. First-principles NMR calculations were performed on the resulting MD structure by use of the CASTEP software package,[41−43] which implements a plane-wave density-functional theory (DFT) approach applicable to periodic systems. NMR shielding calculations utilized the gauge including projector-augmented waves (GIPAW) approach,[42,44,45] with a cutoff energy of 650 eV. Electronic correlation effects were modeled by use of the Perdew−Burke−Ernzerhof (PBE) generalized gradient approximation.[46] The core electrons in U were treated with a scalar relativistic pseudopotential.[47] No spin−orbit (SO) effects were employed for calculation of the ^{1}H NMR chemical shifts. Calculations on model uranyl compounds have shown that the impact of relativistic SO coupling on the predicted chemical shifts is very small for protons located two or more bonds from the U nucleus (Professor Jochen Autschbach, personal communication). To allow comparison to experimental results, the chemical shift δ was derived from the calculated chemical shielding σ_{iso} and a shielding reference σ_{ref} according to the expression $\delta = \sigma_{ref} - \sigma_{iso}$. In previous CASTEP investigations, σ_{ref} was chosen to allow the mean of experimental and calculated chemical shifts to coincide. In the present study, this comparison is complicated by the paucity of experimental ^{1}H chemical shifts for well-defined uranyl compounds. A value of 30.8 ppm for σ_{ref} was employed to provide agreement between the calculated and experiment chemical shift of α-UOH but was slightly larger than σ_{ref} typically reported for organic compounds, $\sigma \approx 30.5$ ppm.[48] A similar trend was noted in a recent CASTEP study of $Ba_2In_2O_4(OH)_2$, including the observation that a reliable set of σ_{ref} parameters still needs to be developed for inorganic materials.[49]

To explore the local U−OH potential energy surfaces, small molecular fragments containing the bridging μ_2-OH motif were extracted from the recently reported U_{24} capsule structures.[31] Subsequent optimization of the water position and structure with different numbers of explicit hydrogen-bonded waters were performed with the Gaussian 09 suite of programs (Gaussian Inc., Wallingford, CT),[50] using DFT and B3LYP methods with the 6-311++G(2d,2p) basis set for O and H, plus the 1997 Stuttgart relativistic small core (RSC) effective core potential (ECP) for U,[51] in both vacuum and with a polarizable continuum model (PCM) water solvent.

3. RESULTS AND DISCUSSION

3.1. Thermogravimetric Analysis and Raman Characterization. TGA analysis of as-synthesized α-$UO_2(OH)_2$ shows minor weight loss below 150 °C due to surface absorption of water (Figure S1, Supporting Information). Significant weight loss starts at around 300 °C and reaches a stable phase near 600 °C, indicating formation of UO_3 (exptl 5.2%, calcd 5.9%). A second weight loss of 1.5% above 600 °C is in agreement with the formation of U_3O_8 (calcd 1.7%) as final product. TGA/DSC for hydrated uranyl hydroxide metaschoepite, $(UO_2)_4O(OH)_6{\cdot}5H_2O$ (Figure S2), revealed the complexity of hydrogen and oxygen environments in this phase. As-synthesized material shows a significant weight loss of 4% at ~110 °C, followed by 1% from 110 to 240 °C, and a final 4.6% until the stable phase of UO_3 is reached at 430 °C. This multistep behavior is similar to previous TGA reports.[8] The first weight loss of 4% is attributed to the loss of interlayer water molecules, which is lower than the calculated water content of 7%. The total loss of 9.5% is close to 11.2%, as expected for the transformation of metaschoepite to UO_3. A further loss of 1.2% from 550 to 620 °C is attributed to formation of U_3O_8 as the final product (calcd 1.6%). On the basis of this result, we can describe the formula as $[(UO_2)_8O_2(OH)_{12}(H_2O)_{10-12}]$.

The Raman spectrum of α-UOH $[\alpha$-$UO_2(OH)_2]$ revealed a single symmetrical peak at 837 cm^{-1} corresponding to the terminal U=O oxygen (Figure S3). This is in good agreement with the crystallographic result, as there is only one independent uranium site and one independent terminal

DOI: 10.1021/acs.jpcc.6b02692
J. Phys. Chem. C 2016, 120, 10675−10685

oxygen site in the structure, with all terminal uranium−oxygen bonds equivalent. The Raman spectrum for metaschoepite (Figure S3) is much more complex. The absorbance for terminal U═O bonds is composed of two distinct peaks centered at 841 and 826 cm^{-1}, as well as a shoulder around 801 cm^{-1}. This is a clear indication of different coordination environments for the multiple uranium sites in metaschoepite structure. The XRD patterns for α-UOH (Figure S4) and metaschoepite (Figure S5) are *consistent* with the reported structures but are not perfect matches. We attribute the discrepancies to both preferred orientation of the layered phase on the sample holder, and the presence of some schoepite material. However, in comparison to all the available phases in the Inorganic Crystal Structure Database (ICSD), these are the best matches. Given the many variations of possible hydration−dehydration steps, there are likely related variations of these phases based on differences in the interlayer water or layer stacking that are not yet completely documented.

3.2. Solid-State ^{1}H NMR. Figure 2 (upper panel) shows the ^{1}H MAS NMR spectrum of α-UOH with a single resonance

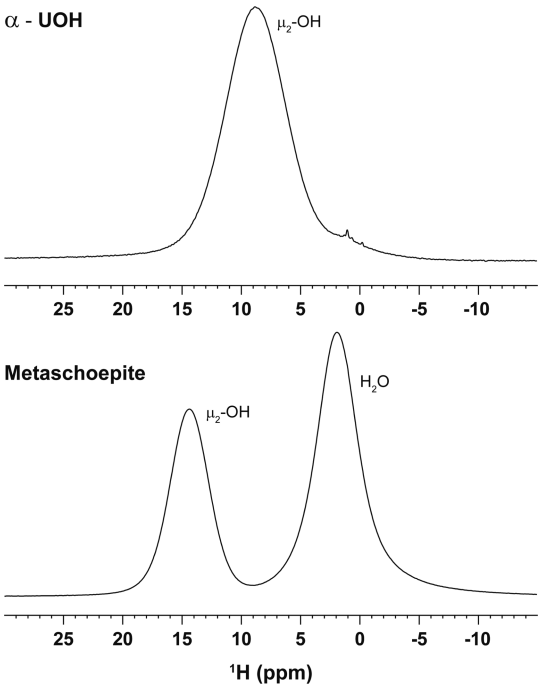

Figure 2. Solid-state ^{1}H MAS NMR spectra (isotropic peak region) for α-$UO_2(OH)_2$ and metaschoepite, $(UO_2)_4O(OH)_6{\cdot}5H_2O$. Sample temperature was 45 °C (set temperature 20 °C).

observed at δ = +8.8 ppm with a full width at half-maximum (fwhm) line width of 3580 Hz. This proton environment was assigned to μ_2-OH hydrogen coordinated to U═O oxygen of the adjacent uranyl polyhedron layer. The +8.8 ppm chemical shift results from the weaker hydrogen-bond strength of this μ-OH proton (see additional discussion in section 3.3). A minor unassigned impurity resonance at δ = +0.9 ppm (2%) was also present. Spectral deconvolution for the entire spinning sideband manifold is shown in Figure S6 and summarized in Table S1. The ^{1}H MAS NMR spectrum of metaschoepite (Figure 2, lower panel) reveals two distinct resonances at δ = +14.4 ppm (35%) with fwhm = 2270 Hz and at δ = +1.9 ppm (65%) with fwhm = 2463 Hz, which were assigned to μ_2-OH and interlayer water protons, respectively. The percentages in parentheses indicate the fraction of the integrated area of each peak. Spectral deconvolutions for metaschoepite are shown in Figure S7. The ^{1}H MAS NMR spectra and assignments are in excellent agreement with those recently reported,[30] even though the μ_2-OH chemical shift in those results appears to be >+16 ppm (the exact δ was not actually reported). The large ^{1}H NMR chemical shift values for μ_2-OH reveal strong hydrogen bonding to the adjacent water (section 3.3), while the reduced chemical shift of the interlayer water reflects the lack or disruption of an extensive water−water hydrogen-bonding network in comparison to the hydrogen-bonding network in bulk water ($\delta \approx$ +4.8 ppm). The ^{1}H NMR resonances are broadened by both residual ^{1}H−^{1}H homonuclear dipolar coupling not averaged by MAS and by distributions in the chemical shifts reflecting heterogeneity of the local hydrogen environment. Experimental observation of two distinct ^{1}H NMR resonances also provides an upper limit on the proton exchange rate between the different environments, requiring the rate to be slow on the NMR time scale ($k \ll \Delta\nu$ = 7450 Hz), where $\Delta\nu$ is the frequency separation between resonances. Variable-temperature ^{1}H MAS NMR of metaschoepite (Figure S8) reveals no major variations in chemical shift or line width. It is important to note that these results support the argument that (i) for the temperature range investigated, the rate of proton exchange between the different water and μ_2-OH environments is slow, and (ii) the interlayer H_2O species do not have rapid dynamics that completely average the ^{1}H−^{1}H dipolar coupling. The experimentally NMR measured μ_2-OH/H_2O proton ratio was 0.54 ± 0.2, which lies between the predicted 0.6 ratio for metaschoepite and the predicted 0.5 ratio for schoepite. This could suggest a mixture of schoepite/metaschoepite phases and is consistent with previous discussions concerning the ease of dehydration of schoepite (even at room temperature in air).[6]

Figure 3 shows the ^{1}H MAS NMR spectra resulting from in-rotor heating of the metaschoepite sample and reveals that additional dehydration processes are occurring. Heating from 100 to 200 °C decreases the relative interlayer water concentration, with the μ-OH/H_2O proton ratio increasing to 0.75 following extensive heating at 200 °C. This loss of H_2O was also reflected in the 4−5% weight loss observed in TGA for this material preparation (section 3.1). The increased μ-OH/H_2O proton ratio, along with comparison of Figures 2 and 3, reveals that heating produces a disordered $UO_2(OH)_2$-type phase following loss of water but does not result in direct formation of α-UOH.[6] Closer inspection of NMR spectra (insets, Figure 3) reveals that there were multiple μ-OH and water environments produced during the 200 °C heat treatment, with overlapping resonances corresponding to the original metaschoepite μ-OH·H_2O hydrogen-bonding environment (δ = +14.4 ppm) and a new μ-OH environment at δ = +11.8 ppm. The original metaschoepite interlayer water species at δ = +1.9 ppm and a new water species at δ = +0.6 ppm were also observed. For these new environments, the μ-OH and H_2O ^{1}H MAS NMR chemical shifts both decreased, reflecting a disruption of the hydrogen-bonding network in comparison to the network present in the original metaschoepite. Further heating to 300 °C produced additional proton environments for both μ-OH and H_2O species (lower inset, Figure 3), with the material beginning to decompose into multiple uranyl phases. Table S1 summarizes the different chemical shifts and relative concentrations for these different observed proton environments. This decomposition may have also been

DOI: 10.1021/acs.jpcc.6b02692
J. Phys. Chem. C 2016, 120, 10675−10685

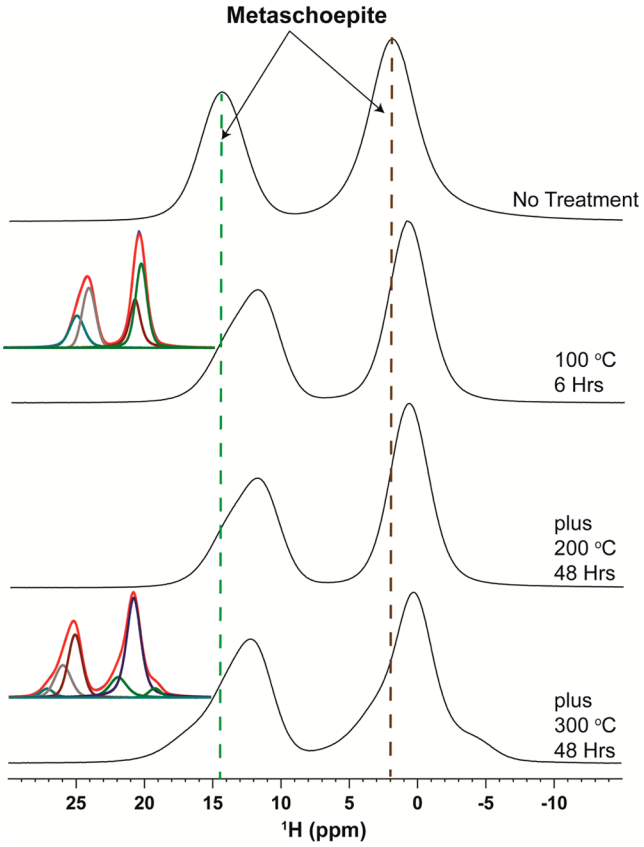

Figure 3. ^{1}H MAS NMR spectra for metaschoepite material following different heat treatments. The colored insets show spectral deconvolutions of the multiple proton environments observed.

accelerated by the mechanical spinning; previous results have shown that the dehydration of metaschoepite can be accelerated by external (mechanical) stresses.[6] These heating studies highlight that dehydration performed directly in the MAS NMR rotor was not successful in producing a single dehydrated uranyl species.

The 2D ^{1}H DQ NMR correlation spectrum for α-UOH is shown in Figure 4 and reveals only a single autocorrelation peak on the diagonal, with no off-diagonal resonances (which is as expected, since there is only a single ^{1}H environment). Observation of the DQ autocorrelation peak reveals the presence of strongly dipolar-coupled protons that are in the same chemical environment (i.e., having the same chemical shift), which is consistent with the 2.62 Å ^{1}H−^{1}H distance in the reported crystal structure. The GIPAW-predicted ^{1}H NMR chemical shift for α-UOH, based on the crystal structure shown in Figure 4, agrees well with the experimental result. It should be noted that the original CIF structure file (9153-ICSD) for α-UOH gives a UO−H bond distance of 0.76 Å, which is unrealistically short. The proton position was allowed to relax within the CASTEP software to give an O−H distance of 0.989 Å prior to the NMR calculation. This new bond length agrees with the ∼1 Å distance suggested in the original structure report.[9]

The 2D ^{1}H DQ NMR correlation spectrum for metaschoepite $(UO_2)_4O(OH)_6{\cdot}5H_2O$ is shown in Figure 5. Off-diagonal correlation peaks arising from through-space ^{1}H−^{1}H dipolar coupling between μ_2-OH and interlayer H_2O proton environments, along with autocorrelation peaks on the diagonal for both proton species, were observed. The XRD crystal structure

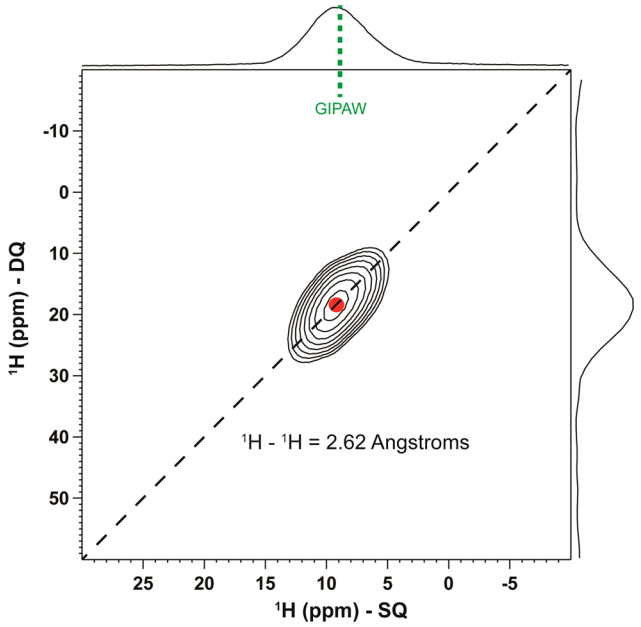

Figure 4. Two-dimensional ^{1}H DQ-SQ NMR correlation spectrum for α-$UO_2(OH)_2$, with a single resonance (solid red circle) observed along the autocorrelation diagonal (---). This peak is produced by ^{1}H−^{1}H dipolar coupling between equivalent proton environments. The GIPAW-predicted ^{1}H NMR chemical shift based on the reported crystal structure (green dotted line) is also shown.

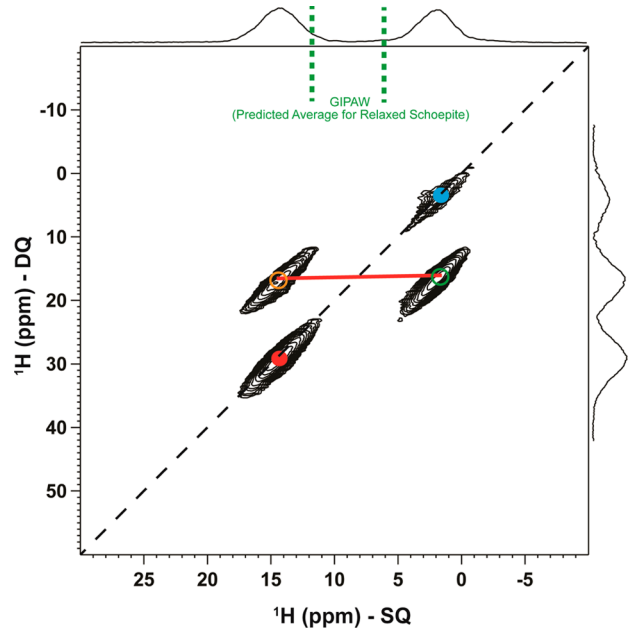

Figure 5. Two-dimensional ^{1}H DQ-SQ NMR correlation spectrum for metaschoepite, $(UO_2)_4O(OH)_6{\cdot}5H_2O$. Resonances along the autocorrelation diagonal (---) result from protons in μ_2-OH (solid red circle) and interlayer water (solid blue circle) environments with ^{1}H−^{1}H dipolar coupling to an equivalent proton type. Off-diagonal cross-peaks (open orange and green circles) result from ^{1}H−^{1}H dipolar coupling between different proton environments. The averaged GIPAW-predicted ^{1}H NMR chemical shifts for the ab initio MD schoepite structure (green dotted line) are also shown.

for metaschoepite could not resolve the individual proton positions,[7] but observation of the ^{1}H NMR DQ correlation suggest that the ^{1}H−^{1}H distances between μ-OH and μ-OH,

DOI: 10.1021/acs.jpcc.6b02692
J. Phys. Chem. C 2016, 120, 10675−10685

between μ-OH and H_2O, and between H_2O and H_2O must all be less than ~3.5 Å to produce the significant $^1H-^1H$ dipolar interactions giving rise to the DQ signal. Since the positions of the protons in metaschoepite have not been reported, direct calculation of the ^1H NMR chemical shifts based on a reported crystal structure was not possible. Ab initio MD studies of hydrogen transfer in schoepite and metaschoepite have been reported by Ostanin and Zeller.[40] We were able to obtain an MD relaxed schoepite structure (Figure 6) in which the interlayer water and μ-OH protons are explicitly resolved, thus allowing for GIPAW chemical shift predictions. The MD snapshot shows significant disorder of the interlayer waters, which leads to multiple chemical shifts for both proton environments. Averaging over all chemical shifts in the MD structure gives $\delta \approx +12$ ppm for the μ_2-OH environment and $\delta \approx +6$ ppm for the interlayer H_2O species (shown in Figure 5). The chemical shift agreement with experiment is marginal: the calculation predicts a smaller μ-OH chemical shift (and smaller hydrogen-bond strength) while predicting a larger chemical shift for the interlayer water. This discrepancy may result from the MD study being carried out for schoepite while the experimental NMR is for a material that is predominantly metaschoepite (which has fewer interlayer waters and stronger predicted hydrogen bonding). Alternatively, the discrepancy may be related to the hydrogen transfer and H_3O^+ formation process targeted by the ab initio MD calculations. Nevertheless, the relative order of the predicted chemical shifts confirms the assignment of μ_2-OH protons and interlayer water protons. The MD structure also predicts intermolecular μ_2-OH $^1H-^1H$ distances of 2.66 and 3.67 Å, consistent with the μ_2-OH experimental 2D DQ NMR autocorrelation peak in Figure 5.

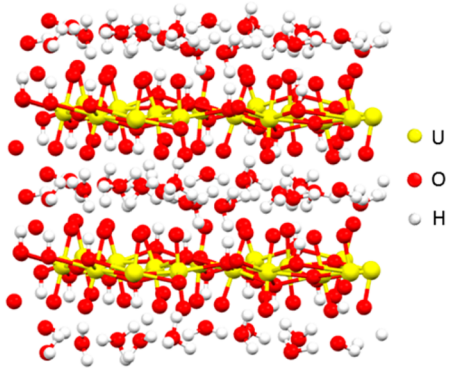

Figure 6. Relaxed schoepite structure obtained from ab initio MD simulations of Ostanin and Zeller,[40] used for CASTEP GIPAW ^1H NMR chemical shift predictions. The proton locations of both μ_2-OH and disordered water allowed the chemical shift of multiple hydrogen-bonding configurations to be evaluated.

3.3. ^1H NMR Chemical Shift Correlations. Because the ab initio MD relaxed schoepite structure has a disordered water structure, it provides many different local bonding configurations that allow relationships between ^1H NMR chemical shifts and hydrogen bonding to be evaluated. Correlations between structure and chemical shifts have been put forward by several groups for both homonuclear and heteronuclear hydrogen bonding, but examples for uranyl oxide-based hydrogen bonding are not available. Variation of ^1H NMR chemical shifts predicted from the CASTEP GIPAW calculations and hydroxyl OH bond length for the relaxed schoepite structure are shown in Figure 7, along with the single point derived from the α-UOH crystal structure.

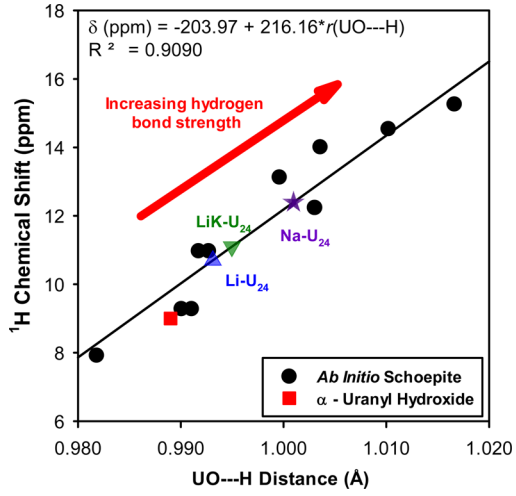

Figure 7. ^1H NMR chemical shift variation with μ_2-O−H bond length from GIPAW predictions for ab initio relaxed schoepite MD structure (black circle) and α-UOH (red square) crystal structure. Estimation of the μ_2-O−H bond distances for U_{24} capsule materials, based on experimental ^1H MAS NMR chemical shifts, are also included (blue triangle, green inverted triangle, and purple star).

While different functional forms for these ^1H NMR chemical shift correlations have been proposed, a linear relationship was defined:

$$^1H\ \delta = -203.97 + 216.16r(\mu_2\text{-O} - \text{H}) \quad (1)$$

Based on eq 1, the experimental ^1H chemical shift of $\delta = +14.4$ ppm for the μ_2-OH proton in metaschoepite (Figure 2) predicts an averaged μ_2-O−H bond length of 1.01 Å, which is longer that the 0.98 Å μ_2O−H bond length in α-UOH. With dehydration of metaschoepite, a new μ_2-OH environment was observed at $\delta = +11.8$ ppm, predicting a shortening of the μ_2-O−H bond length to 0.998 Å. This is consistent with the continued removal of interlayer water and subsequent disruption of the hydrogen-bond network because there is not enough water molecules for all μ_2-OH to be fully hydrogen-bonded. Continued dehydration and complete removal of the interlayer waters will ultimately produce a α-UOH-type bonding configuration, with the weaker hydrogen bond between μ_2-OH and U═O of the adjacent uranyl oxide layer.

3.4. Hydrogen-Bond Strength Correlations. While correlations utilizing a single bond length allow prediction of the ^1H NMR chemical shifts in these uranyl phases, they do not provide many additional structural details of the hydrogen-bonding network. This shortcoming can be addressed by considering the correlation between ^1H NMR chemical shift and local hydrogen-bond strength. In general, the hydrogen-bond geometry in the investigated uranyl bonding environments is described by two distances (r_1 and r_2) and the hydrogen-bond angle θ (Scheme 1).

Hydrogen-bond strength is more often described by the reduced bond coordinates q_1 and q_2:

$$q_1 = \frac{1}{2}(r_1 - r_2) \qquad q_2 = r_1 + r_2 \quad (2)$$

DOI: 10.1021/acs.jpcc.6b02692
J. Phys. Chem. C 2016, 120, 10675−10685

Scheme 1. Hydrogen-Bond Configuration and Definition of Reduced Coordinates q_1 and q_2 in Uranyl Materials

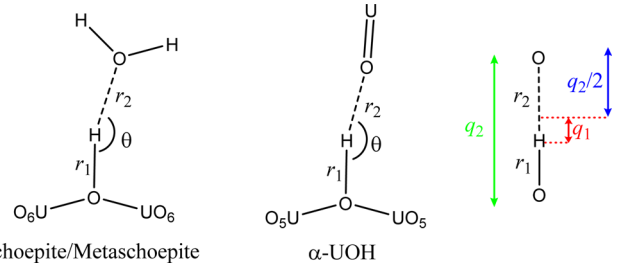

If an approximately linear hydrogen bond is assumed in these materials, q_1 describes the displacement of the hydrogen from the center of the hydrogen-bond potential (asymmetry), and q_2 corresponds to the O···O distance (Scheme 1). In the analysis of ab initio MD relaxed schoepite structure, only two-centered hydrogen bonds (bonded to only two O atoms) that were approximately linear ($165° < \theta \leq 180°$) were used in the analysis. Variation of ^{1}H NMR chemical shift with q_1 displacement is shown in Figure 8. It is first noted that the

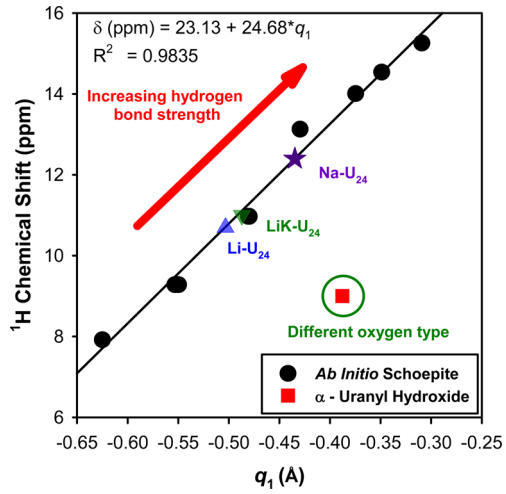

Figure 8. GIPAW-predicted ^{1}H NMR chemical shift variation with hydrogen-bond coordinate q_1 for ab initio relaxed schoepite MD structure (black circles) and α-UOH crystal structure (red squares). Estimation of the q_1 bond coordinate for U_{24} capsule materials, based on experimental ^{1}H MAS NMR chemical shifts, are also included (blue triangle, green inverted triangle, and purple star).

q_1 behavior of the α-UOH ^{1}H chemical shift is very different than the behavior in the relaxed schoepite material. This result is not surprising given that, in the weak hydrogen-bond limit, the q_1 behavior of the ^{1}H chemical shift is impacted to a greater extent by the chemical structure of the two heavy atoms: in this case, hydrogen bonding between μ_2-OH and either a U═O oxygen (in α-UOH) or the oxygen of interlayer water (in schoepite and metaschoepite). Differences in q_1 behavior have previously been noted between oxygen atoms attached to saturated versus unsaturated carbons,[52] as well as the development of different q_1 correlations. Because α-UOH provides only a single ^{1}H chemical shift value, this relationship was not determined. For GIPAW-predicted ^{1}H NMR chemical shifts for the MD relaxed schoepite structure, a linear correlation between ^{1}H chemical shift and q_1 was defined:

$$^1\text{H}\ \delta = 23.13 + 24.68q_1 \quad (3)$$

The negative q_1 observed for all μ_2-OH environments in the relaxed schoepite structure reveals that these protons are displaced from the center of the O···O distance toward μ_2-O. An equally shared proton (i.e., strong hydrogen bond) would have $q_1 = 0$. Increasing the magnitude of q_1 displacement, with the hydrogen closer to μ_2-O, corresponds to diminished hydrogen-bond strengths and a reduced ^{1}H NMR chemical shift (more shielded). The experimental δ = +14.4 ppm ^{1}H chemical shift in metaschoepite predicts an averaged −0.35 Å displacement of the hydrogen from the center of the O···O distance. The δ = +11.8 ppm observed with heating of metaschoepite argues that the hydrogen is further displaced to −0.46 Å. with the subsequent reduction in hydrogen-bonding strength for this uranyl decomposition phase.

Additional structural information can be obtained by relating hydrogen-bond distances to valence bond orders, defined by

$$p_1 = \exp[-(r_1 - r_1^0)/b_1]$$
$$p_2 = \exp[-(r_2 - r_2^0)/b_2] \quad (4)$$

where r_1^0 and r_2^0 represent the equilibrium distances in the O−H and H−O equivalent bonding environment, and b_1 and b_2 are parameters describing the bond valence decay with distance. If the total bond valence of hydrogen is assumed to be unity, it follows that

$$p_1 + p_2 = \exp[-(r_1 - r_1^0)/b_1] + \exp[-(r_2 - r_2^0)/b_2] = 1 \quad (5)$$

Since oxygen is the heavy atom in both bond valences, then $r_1^0 = r_2^0 = r$ and $b_1 = b_2 = b$, which allows simplification of eq 5 to give

$$q_2 = r_1 + r_2 = 2r^0 + 2q_1 + 2b \ln[1 + \exp(-2q_1/b)] \quad (6)$$

Parameter b is defined as

$$b = [q_2^{\min} - 2r^0]/2 \ln 2 \quad (7)$$

where $q_2^{\min}$ represents the minimum possible O···O bond distance (if a linear arrangement is assumed). This relationship for the μ_2-OH···H_2O hydrogen-bond distances, based on the relaxed schoepite structure, is shown in Figure 9. The fit to eq 6 gives r^0 = 0.980 Å and b = 0.302 Å, with a corresponding $q_2^{\min}$ of 2.38 Å. The 0.980 Å distance matches the optimized distance found for α-UOH. The correlation shows that as the O···O distance (q_2) increases (i.e., the water moves away) the extent of displacement of H from the equilibrium hydrogen-bond position (q_1) also increases, corresponding to a weaker hydrogen bond and a subsequent reduction in ^{1}H NMR chemical shift.

3.5. Comparison of μ_2-OH Chemical Shifts between Layered Uranyl Materials and Uranyl Capsule Materials.

In prior studies of $[UO_2(O)_2(OH)]_{24}^{24-}$ (U_{24}) capsules, we reported ^{1}H MAS NMR chemical shifts in materials with different cations: Li−U_{24} (δ = +10.7 ppm), LiK−U_{24} (δ = +11.1 ppm), and Na−U_{24} (δ = +12.4 ppm). These U_{24} chemical shifts are intermediate between those of α-UOH and metaschoepite materials, suggesting the strength of hydrogen bonding between μ_2-OH and neighboring water is also intermediate in comparison to the two layered uranyl phases. Based on the correlations in Figures 8 and 9, the magnitude of hydrogen-bond strength is on the order of Li−U_{24} < LiK−U_{24} < Na−U_{24},

DOI: 10.1021/acs.jpcc.6b02692
J. Phys. Chem. C 2016, 120, 10675−10685

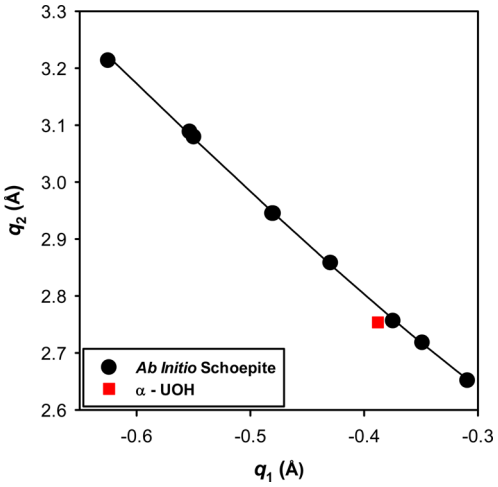

Figure 9. Correlation between reduced hydrogen-bond coordinates q_1 and q_2 for uranyl materials, based on eq 6.

which reflects a ~0.007 Å variation in UO−H bond length or q_1 displacement. Crystal structures of LiK−U_{24} and Na−U_{24} can be used to explain this trend,[29] even though the protons are not crystallographically determined in these structures. For LiK−U_{24}, $^2/_3$ of the μ_2-OH ligands are bonded to a Li^+ cation on the outside of the capsule, where the hydroxyl protons are also located (see Figure 1C).[31] The presence of this Li^+ sterically hinders close association of a hydrogen-bonding water molecule, the Li−O coordination influences the strength of the O−H bond, and Li^+ disrupts the extended water−water hydrogen-bonding network. On average, this produces a weaker μ_2-OH hydrogen bond to water and therefore a smaller ^{1}H NMR chemical shift. In Na−U_{24}, only $^1/_6$ of the μ_2-OH ligands bind a Na^+ cation outside the capsule, and therefore the Na−U_{24} hydroxyls are more available to associate with lattice water via hydrogen bonding. Moreover, for Na−U_{24} every hexagonal face hosts an additional water molecule that is available to hydrogen-bond to all μ_2-OH ligands in the hexagonal opening. LiK−U_{24} also hosts a water molecule in the hexagonal face, but this water is bonded to the encapsulated K^+ and therefore not readily available for association with hydroxyl ligands via hydrogen bonding. The locations of these different species on the outside of the LiK−U_{24} and Na−U_{24} capsules are highlighted in Figure S9. Note there is minimal crystallographic information about the lattice species for Li−U_{24} because they are disordered and probably mobile. We therefore assume, based on the ^{1}H NMR chemical shift, that of the three uranyl U_{24} capsules, the μ_2-OH proton of Li−U_{24} has the strongest cation interactions and correspondingly the weakest hydrogen bonding with lattice water. The impact of direct μ_2-OH and cation (Li^+, Na^+, K^+) coordination on the observed ^{1}H NMR chemical shift has not yet been explicitly determined. Current research efforts in our laboratories are exploring these effects in detail for Li−U_{24} and Na−U_{24} materials, with the goal of combining the ^{1}H and ^{7}Li (or ^{23}Na) NMR chemical shift data to extract additional structural details for these capsules. These experiments will be reported in a later publication.

Variations of the μ_2-OH hydrogen-bonding strength in the U_{24} materials resulting from differences in the water lattice interactions were also supported by ab initio calculations on small uranyl peroxide clusters (dimer fragments) as shown in Figure 10. The potential energy surface as a function of UO−H bond length revealed that, in general, the presence of an explicit water species directly hydrogen-bonded to μ_2-OH lengthens the O−H bond length in comparison to simple use of an implicit polarizable continuum model (PCM) solvent dielectric. For structures obtained by use of only a PCM solvent, the energy minimum corresponds to a O−H bond length of

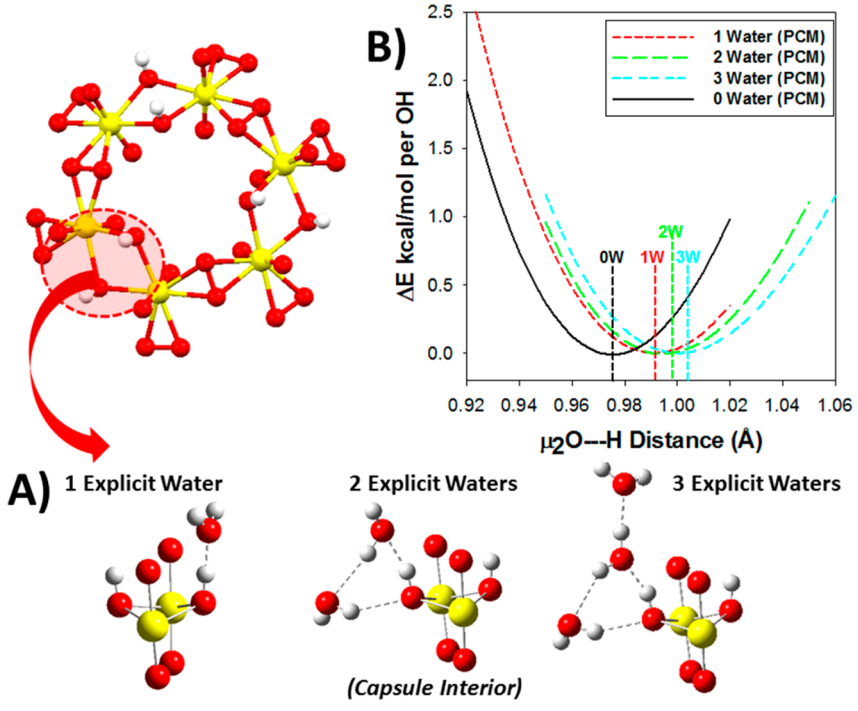

Figure 10. (A) Representations of optimized small uranyl peroxide cluster fragments extracted from the larger U_{24} uranyl capsule structure with different numbers of explicit waters. Hydrogen bonds involving the waters are shown as dashed lines. In the U_{24} structures, the μ_2-OH are oriented with the hydrogens pointed to the capsule exterior. (B) Variation of energy for these optimized structures as a function of μ_2O−H bond length.

DOI: 10.1021/acs.jpcc.6b02692
J. Phys. Chem. C 2016, 120, 10675−10685

~0.975 Å, consistent with the 0.977 Å distance recently reported for the computationally optimized U_{24} capsule structure.[31] When one explicit water (combined with a PCM solvent) was included during the cluster optimization, the low-energy structure has a μ_2-O−H bond length of ~0.99 Å, reflecting the hydrogen bond between water and μ_2-OH ligand. The increased bond length would result in a larger ^{1}H NMR chemical shift (Figures 7 and 8). The presence of two explicit water molecules hydrogen-bonded to the μ_2-OH ligand, including a water environment located toward the center of the hexagonal face, further displaced the low-energy μ_2-O−H bond distance to ~0.998 Å. The presence of three explicit waters in these optimized uranyl clusters predicted an additional lengthening of the μ_2-O−H bond length to ~1.005 Å. While we do not claim that these represent the actual local water structures present in the U_{24} capsule materials, it is clear that increasing the degree of water-based hydrogen bonding produced a lengthening of the μ_2-O−H bond and correspondingly an increase in the ^{1}H NMR chemical shift. Interestingly, the range of optimized μ_2-O−H bond lengths matches nicely with the distances predicted from experimentally observed ^{1}H MAS NMR results (Figure 7).

For the U_{24} capsules, the presence of significant, strong μ_2-OH hydrogen bonding to water may also be related to the lack of deprotonation behavior of these hydroxyl ligands within the clusters. Previous MD simulations[40] provide some insight into the hydrogen-transfer process for these hydrogen-bonded networks. While H was observed to readily leave the μ_2O ligand during simulations, the lifetime of the subsequently formed H_3O^+ species was very short (<20 fs). Thus, the H rapidly recombines with the original μ_2O group, resulting in the proton not being transferred to other O species (including transfer of H to other water molecules). This is consistent with the lack of exchange averaging of the μ_2-OH resonances in the ^{1}H MAS NMR for both metaschoepite and U_{24} capsules. It is argued that increasing the lifetime of the H_3O^+ intermediate, by either changes in chemistry or increased temperatures, could ultimately lead to H exchange in the solid state on the NMR time scale.

4. CONCLUSIONS

Solid-state ^{1}H MAS NMR spectroscopy has been utilized to investigate local proton environments in layered uranyl materials that are anhydrous (α-UOH) and in compounds containing interlayer water (schoepite/metaschoepite). These results were used to interpret the prior reported ^{1}H MAS NMR of the uranyl peroxide/hydroxide U_{24} capsules. For metaschoepite, the use of MAS allowed both μ_2-OH and interlayer water species to be resolved and quantified in ^{1}H NMR spectra. Two-dimensional DQ ^{1}H NMR correlation experiments revealed that, for α-UOH, strong ^{1}H−^{1}H dipolar coupling between the hydroxyl protons exists and is consistent with the known crystal structure. For metaschoepite, there is significant ^{1}H−^{1}H dipolar coupling between the hydroxyl proton and the interlayer water species and also dipolar coupling between protons in the interlayer water. These NMR results demonstrate that there is an extensive hydrogen-bonded network present in these materials and that the water dynamics are slow on both the dipolar and chemical shift NMR time scales. Correlations between ^{1}H NMR chemical shift and μ_2-O−H bond length as well as the q_1 hydrogen-bond strength parameter were developed. These results demonstrate that, for α-UOH, the hydrogen-bond strength between μ_2OH and U=O of the adjacent uranyl layer is weak, while in metaschoepite the hydrogen bonding between μ_2-OH and oxygen of interlayer water is significantly stronger. These ^{1}H NMR chemical shift correlations predict an optimal hydrogen-bond length of 0.980 Å for μ_2-OH to interlayer water, with deviations from this distance reflecting changes in hydrogen bonding. Variation of the ^{1}H NMR chemical shift during dehydration of metaschoepite reveals a disruption of the average hydrogen-bond strengths with the removal of interlayer water species, along with formation of multiple mixed phases at higher temperatures. For U_{24} uranyl capsules, the relative strength of the μ_2-OH to water hydrogen bond was determined to be Li−U_{24} < LiK−U_{24} < Na−U_{24}, which reflected disruption of the hydrogen-bonding network produced by changes in cation coordination. These results reveal the utility of ^{1}H MAS NMR to directly monitor changing hydrogen-bonding environments in uranyl materials and to predict hydration states on the basis of NMR chemical shift.

■ ASSOCIATED CONTENT

Supporting Information

The Supporting Information is available free of charge on the ACS Publications website at DOI: 10.1021/acs.jpcc.6b02692.

Nine figures and one table with TGA/DSC, Raman, XRD, and variable-temperature ^{1}H MAS NMR characterization of α-UOH and metaschoepite materials (PDF)

■ AUTHOR INFORMATION

Corresponding Author

*Phone +1-505-844-1225; fax +1-505-844-2974; e-mail tmalam@sandia.gov.

Notes

The authors declare no competing financial interest.

■ ACKNOWLEDGMENTS

Sandia is a multiprogram laboratory operated by Sandia Corporation, a Lockheed Martin Company, of the United States Department of Energy's National Nuclear Security Administration under Contract DE-AC04-94AL85000. The work at Oregon State University was funded by the Materials Science of Actinides, an Energy Frontier Research Center funded by the Department of Energy, Office of Science, Office of Basic Energy Sciences under Award DE-SC0001089. We are also indebted to Professor Sergey Ostanin for providing the ab initio relaxed schoepite structure from ref 40, used for GIPAW NMR calculations.

■ REFERENCES

(1) *Fuel Cycle Stewardship in a Nuclear Renaissance*; The Royal Society Science Policy Centre Report 10/11, London, 2011; https://royalsociety.org/~/media/Royal_Society_Content/policy/projects/nuclear-non-proliferation/FuelCycleStewardshipNuclearRenaissance.pdf.

(2) Baker, R. J. Uranium Minerals and their Relevance to Long Term Storage of Nuclear Fuels. *Coord. Chem. Rev.* **2014**, *266−267*, 123−136.

(3) Corbel, C.; Sattonnay, G.; Guilbert, S.; Garrido, F.; Barthe, M. F.; Jegou, C. Addition Versus Radiolytic Production Effects of Hydrogen Peroxide on Aqueous Corrosion of UO_2. *J. Nucl. Mater.* **2006**, *348*, 1−17.

(4) Sowder, A. G.; Clark, S. B.; Fjeld, R. A. The Transformation of Uranyl Oxide Hydrates: The Effect of Dehydration on Synthetic

DOI: 10.1021/acs.jpcc.6b02692
J. Phys. Chem. C 2016, 120, 10675−10685

Metaschoepite and Its Alteration to Becquerelite. *Environ. Sci. Technol.* **1999**, *33*, 3552−3557.
(5) Finch, R. J.; Cooper, M. A.; Hawthorne, F. C.; Ewing, R. C. The Crystal Structure of Schoepite, $[(UO_2)_8O_2(OH)_{12}](H_2O)_{12}$. *Can. Mineral.* **1996**, *34*, 1071−1088.
(6) Finch, R. J.; Hawthorne, F. C.; Ewing, R. C. Structural Relationships Among Schoepite, Metaschoepite and "Dehydrated Schoepite". *Can. Mineral.* **1998**, *36*, 831−845.
(7) Weller, M. T.; Light, M. E.; Gelbrich, T. Structure of Uranium(VI) Oxide Dihydrate, $UO_3{\bullet}2H_2O$; Synthetic Meta-Schoepite $(UO_2)_4O(OH)_6{\bullet}5H_2O$. *Acta Crystallogr., Sect. B: Struct. Sci.* **2000**, *56*, 577−583.
(8) Brugger, J.; Meisser, N.; Etschmann, B.; Ansermet, S.; Pring, A. Paulscherrerite from the Number 2 Workings, Mount Painter Inlier, Northern Flinders Ranges, South Australia: "Dehydrated Schoepite" is a Mineral After All. *Am. Mineral.* **2011**, *96*, 229−240.
(9) Taylor, J. The Structure of the α Form of Uranyl Hydroxide. *Acta Crystallogr., Sect. B: Struct. Crystallogr. Cryst. Chem.* **1971**, *27*, 1088−1091.
(10) Allen, P. G.; Bucher, J. J.; Clark, D. L.; Edelstein, N. M.; Ekberg, S. A.; Gohdes, J. W.; Hudson, E. A.; Kaltsoyannis, N.; Lukens, W. W.; et al. Multinuclear NMR, Raman, EXAFS, and X-ray Diffraction Studies of Uranyl Carbonate Complexes in Near-Neutral Aqueous Solution. X-ray Structure of $[C(NH_2)_3]_6[(UO_2)_3(CO_3)_6]{\bullet}6.5H_2O$. *Inorg. Chem.* **1995**, *34*, 4797−4807.
(11) Brucher, E.; Glaser, J.; Toth, I. Carbonate Exchange for the Complex $UO_2(CO_3)_3^{4-}$ in Aqueous Solution as Studied by ^{13}C NMR Spectroscopy. *Inorg. Chem.* **1991**, *30*, 2239−2241.
(12) Finch, R. J.; Ewing, R. C. Clarkeite: New Chemical and Structural Data. *Am. Mineral.* **1997**, *82*, 607−619.
(13) Gong, C.-M. S.; Poineau, F.; Czerwinski, K. R. Synthesis and Characterization of the Solid Uranium(VI) Dioxo-Diacetohydroxamate Complex. *Radiochim. Acta* **2007**, *95*, 439−450.
(14) Chen, C.-S.; Kao, H.-M.; Lii, K.-H. $K_5(UO_2)_2[Si_4O_{12}(OH)]$: A Uranyl Silicate Containing Chains of Four Silicate Tetrahedra Linked by SiO···HOSi Hydrogen Bonds. *Inorg. Chem.* **2005**, *44*, 935−940.
(15) Moll, H.; Reich, T.; Szabó, Z. The Hydrolysis of Dioxouranium-(VI) Investigated Using EXAFS and ^{17}O-NMR. *Radiochim. Acta* **2000**, *88*, 411.
(16) Clark, D. L.; Conradson, S. D.; Donohoe, R. J.; Keogh, D. W.; Morris, D. E.; Palmer, P. D.; Rogers, R. D.; Tait, C. D. Chemical Speciation of the Uranyl Ion under Highly Alkaline Conditions. Synthesis, Structures, and Oxo Ligand Exchange Dynamics. *Inorg. Chem.* **1999**, *38*, 1456−1466.
(17) Szabó, Z.; Grenthe, I. Reactivity of the "yl"-Bond in Uranyl(VI) Complexes. 1. Rates and Mechanisms for the Exchange between the Trans-Dioxo Oxygen Atoms in $(UO_2)_2(OH)_2^{2+}$ and Mononuclear $UO_2(OH)_n^{2-n}$ Complexes with Solvent Water. *Inorg. Chem.* **2007**, *46*, 9372−9378.
(18) Aaberg, M.; Ferri, D.; Glaser, J.; Grenthe, I. Structure of the Hydrated Dioxouranium(VI) Ion in Aqueous Solution. An X-ray Diffraction and Proton NMR Study. *Inorg. Chem.* **1983**, *22*, 3986−3989.
(19) Banyai, I.; Glaser, J.; Micskei, K.; Toth, I.; Zekany, L. Kinetic Behavior of Carbonate Ligands with Different Coordination Modes: Equilibrium Dynamics for Uranyl(2+) Carbonato Complexes in Aqueous Solution. A ^{13}C and ^{17}O NMR Study. *Inorg. Chem.* **1995**, *34*, 3785−3796.
(20) Nyman, M.; Rodriguez, M. A.; Alam, T. M. The U28 Nanosphere: What's Inside? *Eur. J. Inorg. Chem.* **2011**, *2011*, 2197−2205.
(21) Nyman, M.; Alam, T. M. Dynamics of Uranyl Peroxide Nanocapsules. *J. Am. Chem. Soc.* **2012**, *134*, 20131−20138.
(22) Azenha, M. E. D. G.; Burrows, H. D.; Formosinho, S. J.; Leitao, M. L. P.; Miguel, M.d. G. M. Co-ordination Behaviour of Dioxouranium(VI) Nitrate in Water-Acetone Mixtures. *J. Chem. Soc., Dalton Trans.* **1988**, 2893−2895.
(23) Bardin, N.; Rubini, P.; Madie, C. Hydration of Actinyl(VI), $MO_2^{+2}{}_{aq}$ (M = U, Np, Pu). An NMR Study. *Radiochim. Acta* **1998**, *83*, 189−194.
(24) Weller, M. T.; Dickens, P. G. Pulsed NMR Study of Proton Motions in Uranium Trioxide Hydrates. *J. Solid State Chem.* **1988**, *75*, 141−146.
(25) Porte, A. L.; Gutowsky, H. S.; Boggs, J. E. Proton Magnetic Resonance Studies of Polycrystalline Uranium Oxide Hydrates. I. β-$UO_3 \bullet 2H_2O$. *J. Chem. Phys.* **1962**, *36*, 1695−1699.
(26) Porte, A. L.; Gutowsky, H. S.; Boggs, J. E. Proton Magnetic Resonance Studies of Polycrystalline Uranium Oxide Hydrates. II. β-$UO_3{\bullet}H_2O$. *J. Chem. Phys.* **1962**, *36*, 1700−1703.
(27) Porte, A. L.; Gutowsky, H. S.; Boggs, J. E. Proton Magnetic Resonance Studies of Polycrystalline Uranium Oxide Hydrates. III. $UO_4{\bullet}2H_2O$. *J. Chem. Phys.* **1962**, *37*, 2318−2322.
(28) Chen, C.-S.; Chiang, R.-K.; Kao, H.-M.; Lii, K.-H. High-Temperature, High-Pressure Hydrothermal Synthesis, Crystal Structure, and Solid-State NMR Spectroscopy of $Cs_2(UO_2)(Si_2O_6)$ and Variable-Temperature Powder X-ray Diffraction Study of the Hydrate Phase $Cs_2(UO_2)(Si_2O_6){\cdot}0.5H_2O$. *Inorg. Chem.* **2005**, *44*, 3914−3918.
(29) Alam, T. M.; Liao, Z.; Zakharov, L. N.; Nyman, M. Solid-State Dynamics of Uranyl Polyoxometalates. *Chem. - Eur. J.* **2014**, *20*, 8302−8307.
(30) Odoh, S. O.; et al. Structure and Reactivity of X-ray Amorphous Uranyl Peroxide, U_2O_7. *Inorg. Chem.* **2016**, *55*, 3541−3546.
(31) Miro, P.; Vlaisavljevich, B.; Gil, A.; Burns, P.; Nyman, M.; Bo, C. Self-assembly of Uranyl-peroxide Nanocapsules in Basic Peroxidic Environments. *Chem. - Eur. J.* **2016**, in press.
(32) Liao, Z.; Deb, T.; Nyman, M. Elucidating Self-Assembly Mechanisms of Uranyl−Peroxide Capsules from Monomers. *Inorg. Chem.* **2014**, *53*, 10506−10513.
(33) McGrail, B. T.; Sigmon, G. E.; Jouffret, L. J.; Andrews, C. R.; Burns, P. C. Raman Spectroscopic and ESI-MS Characterization of Uranyl Peroxide Cage Clusters. *Inorg. Chem.* **2014**, *53*, 1562−1569.
(34) Nyman, M.; Burns, P. C. A Comprehensive Comparison of Transition-Metal and Actinyl Polyoxometalates. *Chem. Soc. Rev.* **2012**, *41*, 7354−7367.
(35) Dawson, J. K.; Wait, E.; Alcock, K.; Chilton, D. R. Some Aspects of the System Uranium Trioxide-Water. *J. Chem. Soc.* **1956**, *0*, 3531−3540.
(36) Bielecki, A.; Burum, D. P. Temperature Dependence of ^{207}Pb MAS Spectra of Solid Lead Nitrate. An Accurate, Sensitive Thermometer for Variable-Temperature MAS. *J. Magn. Reson., Ser. A* **1995**, *116*, 215−220.
(37) Takahashi, T.; Kawashima, H.; Sugisawa, H.; Baba, T. ^{207}Pb Chemical Shift Thermometer at High Temperature for Magic Angle Spinning Experiments. *Solid State Nucl. Magn. Reson.* **1999**, *15*, 119−123.
(38) Schnell, I.; Spiess, H. W. High-Resolution ^1H NMR Spectroscopy in the Solid State: Very Fast Sample Rotation and Multiple-Quantum Coherences. *J. Magn. Reson.* **2001**, *151*, 153−227.
(39) Massiot, D.; Fayon, F.; Capron, M.; King, I.; Le Calvé, S.; Alonso, B.; Durand, J. O.; Bujoli, B.; Gan, Z.; Hoatson, G. Modelling One and Two-Dimensional Solid-State NMR Spectra. *Magn. Reson. Chem.* **2002**, *40*, 70−76.
(40) Ostanin, S.; Zeller, P. Ab Initio Study of the Uranyl Oxide Hydrates: a Proton Transfer Mediated by Water. *J. Phys.: Condens. Matter* **2007**, *19*, No. 246108.
(41) Clark, S. J.; Segall, M. D.; Pickard, C. J.; Hasnip, P. J.; Probert, M. I. J.; Refson, K.; Payne, M. C. First Principles Methods Using CASTEP. *Z. Kristallogr. - Cryst. Mater.* **2005**, *220*, 567−570.
(42) Bonhomme, C.; et al. First-Principles Calculation of NMR Parameters Using the Gauge Including Projector Augmented Wave Method: A Chemist's Point of View. *Chem. Rev.* **2012**, *112*, 5733−5779.
(43) Segall, M. D.; Lindan, P. J. D.; Probert, M. J.; Pickard, C. J.; Hasnip, P. J.; Clark, S. J.; Payne, M. C. First-Principles Simulation: Ideas, Illustrations and the CASTEP Code. *J. Phys.: Condens. Matter* **2002**, *14*, 2717−2744.

DOI: 10.1021/acs.jpcc.6b02692
J. Phys. Chem. C 2016, 120, 10675−10685

(44) Pickard, C. J.; Mauri, F. All-Electron Magnetic Response with Pseudopotentials: NMR Chemical Shifts. *Phys. Rev. B: Condens. Matter Mater. Phys.* **2001**, *63*, No. 245101.
(45) Yates, J. R.; Pickard, C. J.; Mauri, F. Calculation of NMR Chemical Shifts for Extended Systems Using Ultrasoft Pseudopotentials. *Phys. Rev. B: Condens. Matter Mater. Phys.* **2007**, *76*, No. 024401.
(46) Perdew, J. P.; Burke, K.; Ernzerhof, M. Generalized Gradient Approximation Made Simple. *Phys. Rev. Lett.* **1996**, *77*, 3865−3868.
(47) Yates, J. R.; Pickard, C. J.; Payne, M. C.; Mauri, F. Relativistic Nuclear Magnetic Resonance Chemical Shifts of Heavy Nuclei with Pseudopotentials and the Zeroth-Order Regular Approximation. *J. Chem. Phys.* **2003**, *118*, 5746−5753.
(48) Asakura, T.; Suzuki, Y.; Yazawa, K.; Aoki, A.; Nishiyama, Y.; Nishimura, K.; Suzuki, F.; Kaji, H. Determination of Accurate ^{1}H Positions of (Ala-Gly)n as a Sequential Peptide Model of Bombyx mori Silk Fibroin before Spinning (Silk I). *Macromolecules* **2013**, *46*, 8046−8050.
(49) Dervişoğlu, R.; Middlemiss, D. S.; Blanc, F.; Lee, Y.-L.; Morgan, D.; Grey, C. P. Joint Experimental and Computational ^{17}O and ^{1}H Solid State NMR Study of $Ba_2In_2O_4(OH)_2$ Structure and Dynamics. *Chem. Mater.* **2015**, *27*, 3861−3873.
(50) Frisch, M. J., et al. *Gaussian 09*; Gaussian, Inc., Wallingford, CT, 2009.
(51) Dolg, M.; Stoll, H.; Preuss, H.; Pitzer, R. M. Relativistic and Correlation Effects for Element 105 (Hahnium, Ha): A Comparative Study of M and MO (M = Nb, Ta, Ha) Using Energy-Adjusted Ab Initio Pseudopotentials. *J. Phys. Chem.* **1993**, *97*, 5852−5859.
(52) Limbach, H.-H.; Tolstoy, P. M.; Pérez-Hernández, N.; Guo, J.; Shenderovich, I. G.; Denisov, G. S. OHO Hydrogen Bond Geometries and NMR Chemical Shifts: From Equilibrium Structures to Geometric H/D Isotope Effects, with Applications for Water, Protonated Water, and Compressed Ice. *Isr. J. Chem.* **2009**, *49*, 199−216.

DOI: 10.1021/acs.jpcc.6b02692
J. Phys. Chem. C 2016, 120, 10675−10685